catalysts

MDPI

Article

Preparation of Rh/Ni Bimetallic Nanoparticles and Their Catalytic Activities for Hydrogen Generation from Hydrolysis of KBH_4

Liqiong Wang [1], Liang Huang [1,*], Chengpeng Jiao [1,2], Zili Huang [2], Feng Liang [3], Simin Liu [3], Yuhua Wang [4] and Haijun Zhang [1,*]

1 The State Key Laboratory of Refractories and Metallurgy, Wuhan University of Science and Technology, Wuhan 430081, China; wlq1823688@sina.com (L.W.); jcp1990@sina.cn (C.J.)
2 Hubei Key Laboratory for Efficient Utilization and Agglomeration of Metallurgical Mineral Resources, Wuhan University of Science and Technology, Wuhan 430081, China; huangzili0424@sina.com
3 School of Chemistry and Chemical Engineering, Wuhan University of Science and Technology, Wuhan 430081, China; feng_liang@whu.edu.cn (F.L.); liusimin@wust.edu.cn (S.L.)
4 Hubei Province Key Laboratory of Science in Metallurgical Process, Wuhan University of Science and Technology, Wuhan 430081, China; Wyh61@163.com
* Correspondence: zhanghaijun@wust.edu.cn (H.Z.); huangliang1986@wust.edu.cn (L.H.); Tel.: +86-027-6886-2829 (H.Z.); +86-027-6886-2258 (L.H.)

Academic Editor: Rajendra S. Ghadwal
Received: 20 March 2017; Accepted: 18 April 2017; Published: 23 April 2017

Abstract: ISOBAM–104 protected Rh/Ni bimetallic nanoparticles (BNPs) of 3.1 nm in diameter were synthesized by a co–reduction method with a rapid injection of KBH_4 solution. The catalytic activities of as–prepared BNPs for hydrogen generation from hydrolysis of a basic KBH_4 solution were evaluated. Ultraviolet–visible spectrophotometry (UV–Vis), transmission electron microscopy (TEM), and high–resolution transmission electron microscopy (HRTEM) were employed to characterize the structure, particle size, and chemical composition of the resultant BNPs. Catalytic activities for hydrolysis of KBH_4 and catalytic kinetics of prepared BNPs were also investigated. It was shown that Rh/Ni BNPs displayed much higher catalytic activities than that of Rh or Ni monometallic nanoparticles (MNPs), and the prepared $Rh_{10}Ni_{90}$ BNPs possessed the highest catalytic activities with a value of 11580 mol–H_2·h^{-1}·mol–Rh^{-1}. The high catalytic activities of Rh/Ni BNPs could be attributed to the electron transfer effect between Rh and Ni atoms, which was confirmed by a density functional theory (DFT) calculation. The apparent activation energy for hydrogen generation of the prepared $Rh_{10}Ni_{90}$ BNPs was about 47.2 ± 2.1kJ/mol according to a kinetic study.

Keywords: Rh/Ni BNPs; hydrogen generation; catalytic activities; electron transfer effect

1. Introduction

Hydrogen is one of many potential alternatives to replace nonrenewable fuel sources that are used nowadays, as it is an environmentally–friendly and renewable energy carrier. However, the technique for hydrogen storage is still a large problem which hinders the application of hydrogen. To date, an extensive body of research has been published on hydrogen storage including liquid hydrogen storage, high pressure gaseous hydrogen storage, adsorption hydrogen storage, metal hydride hydrogen storage, organic compounds hydrogen storage, and liquid phase chemical hydrogen storage [1–4]. Among these methods, liquid phase chemical hydrogen storage attracted considerable attention due to their high hydrogen content, high hydrogen purity, and easy control of the hydrogen generation rate [5,6]. Compared with other chemical hydrogen storage materials (such as hydrazine hydrate, ammonia borane and formic acid), potassium/sodium borohydride (KBH_4/$NaBH_4$) is

more competitive because of several advantages, including safe production process, convenience of transportation, and environmentally benign hydrolysis product $NaBO_2$. However, the rate of hydrogen generation from hydrolysis of $KBH_4/NaBH_4$ aqueous solution is usually low at elevated pH, especially under alkaline conditions, such as pH = 12 [7–9]. Therefore, catalysts are important for hydrolysis of KBH_4, as shown in formula (1):

$$KBH_4 + 2H_2O \xrightarrow{\text{Catalyst}} KBO_2 + 4H_2 \quad (1)$$

It is well–known that nanoparticles (NPs), especially noble metal NPs, can act as high–efficiency catalysts for hydrogen generation from hydrolysis of $KBH_4/NaBH_4$. Moreover, combinations of non–noble metal can reduce the use of noble metals and lower the cost of catalysts. Further, it can also improve the catalytic activities of the catalysts due to the synergistic effect between different metal atoms [9–19]. Our previous work has indicated that alloy–structured $Au_{50}Ni_{50}$ bimetallic nanoparticles (BNPs) exhibited catalytic activities several times higher for hydrogen generation from hydrolysis of $NaBH_4$ aqueous solution, compared with that of Au and Ni monometallic nanoparticles (MNPs) [12]. Au/Co BNPs also displayed a much higher catalytic activity for hydrogen generation than that of Au and Co MNPs [13].

Rh NPs have attracted considerable attention in the catalysis area because they are active for many chemical reactions [20]. For example, Rh NPs supported on silica–coated magnetite showed significant hydrogenation activity of benzene and cyclohexene, and the catalytic activity remained unchangeable for up to 20 cycles [21]. Poly (*N*–vinyl–2–pyrrolidone)–protected Ru/Rh BNPs can act as highly efficient catalysts in the hydrolysis of ammonia borane for hydrogen generation [22]. Ni@(RhNi–alloy) nanocomposites supported on NiAl–layered double hydroxides (NiAl–LDHs) were reported to be highly efficient catalysts towards hydrogen generation in the hydrolysis of $N_2H_4BH_3$ [23]. The addition of Rh metals has greatly improved the catalytic activity of Co–based catalysts in the ethanol stream reforming reaction, indicating the second metal could fundamentally influence the properties of the catalyst [24,25]. Nevertheless, the high cost of Rh hinders its wide industrial application. Thus, a combination of non–noble metal with Rh is a promising strategy for the development of Rh–based catalyst for hydrogen generation [23,26].

In the present paper, a series of ISOBAM–104 (poly (isobutylene–alt–maleic anhydride) $(C_8H_{10}O_3)_m(C_8H_{16}O_3N_2)_i$, designed as ISOBAM–104) protected Rh/Ni BNPs were prepared by a facile method, and the relationship between compositions and structures of the BNPs on their catalytic activities for hydrogen generation were also investigated. ISOBAM–104 is expected to protect the metal NPs from agglomeration because it has numerous of functional groups and can act as chelant. The apparent activation energy of $Rh_{10}Ni_{90}$ BNPs for hydrolysis of KBH_4 aqueous solution was calculated by the Arrhenius method. Moreover, the correlation between catalytic activities of Rh/Ni BNPs and their electronic properties was established based on a density functional theory (DFT) calculation.

2. Results and Discussion

2.1. Structure and Catalytic Activities of Rh/Ni Bimetallic Nanoparticles (BNPs)

Ultraviolet–visible spectrophotometry (UV–Vis) spectra of as–prepared colloidal dispersion are shown in Figure 1. There is no surface plasmon resonance (SPR) peak of Rh, Ni MNPs or Rh/Ni BNPs in measuring range, which is consistent with previous reports [9,18]. The spectra of aqueous dispersed Rh/Ni BNPs displays featureless absorbance that monotonically increase toward a higher Rh content. The absorbance spectra of all BNPs lie between the spectrum of Rh and Ni MNPs, and the obvious differences in absorbance between as–prepared BNPs with varied Rh content suggest that alloy–structured Rh/Ni BNPs were formed.

Figure 2 presents a set of transmission electron microscopy (TEM) micrographs of the prepared Rh, Ni MNPs and Rh/Ni BNPs. The individual NPs appear to be separated uniformly without obvious agglomeration. The average particle sizes of Rh, $Rh_{90}Ni_{10}$, $Rh_{70}Ni_{30}$, $Rh_{30}Ni_{70}$, $Rh_{10}Ni_{90}$ and Ni NPs based on size distribution analysis are about 1.9 ± 0.9 nm, 3.5 ± 1.9 nm, 3.7 ± 1.9 nm, 2.7 ± 0.8 nm, 2.7 ± 0.9 nm and 3.5 ± 1.2 nm, respectively. The elemental ratio of $Rh_{70}Ni_{30}$ BNPs at the selected square in Figure 3 was measured by mapping energy dispersion X–ray spectroscopy (EDS), and it indicates that the compositions of as–prepared $Rh_{70}Ni_{30}$ BNPs are similar to their feeding ratio.

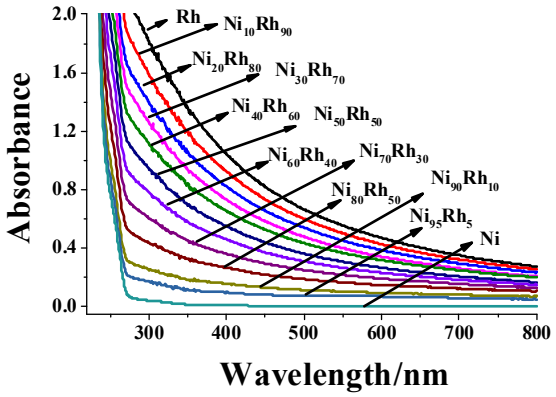

Figure 1. Ultraviolet–visible spectrophotometry (UV–Vis) spectra of colloidal dispersions of $Rh_{(100-x)}Ni_x$ nanoparticles (NPs)(x = 0, 10, 20, 30, 60, 80, 90 and 100) (R_{ISO} = 40, R_{ISO} presents the molar ratio of ISOBAM–104 in alkaline solution to the total metals in the colloidal catalyst mixture; C_{Metal} = 0.66 mM, reduced under ice–water bath for 1 h.).

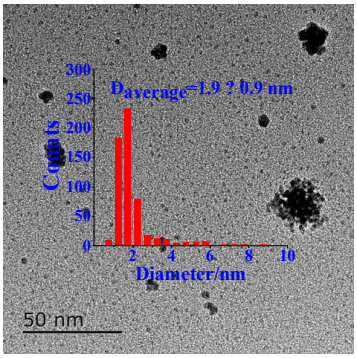

Rh

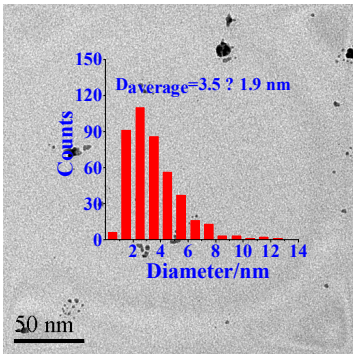

$Rh_{90}Ni_{10}$

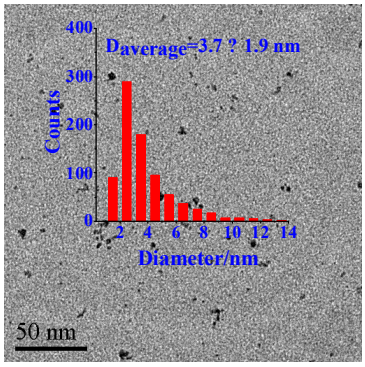

$Rh_{70}Ni_{30}$

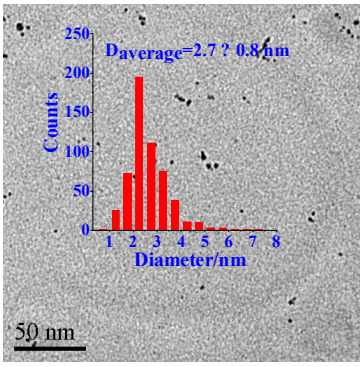

$Rh_{30}Ni_{70}$

Figure 2. *Cont.*

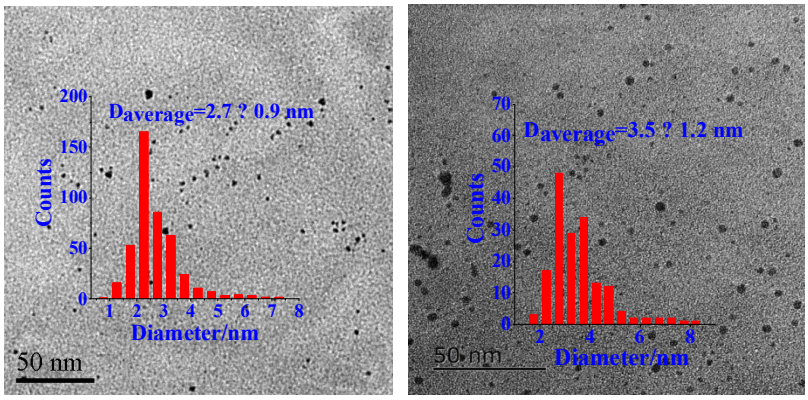

$Rh_{10}Ni_{90}$ Ni

Figure 2. Transmission electron microscopy (TEM) images and size distribution histograms of colloidal dispersions of $Rh_{(100-x)}Ni_x$ (x = 0, 10, 30, 70, 90 and 100) NPs (R_{ISO} = 40, C_{Metal} = 0.66 mM, reduced under ice–water bath for 1h).

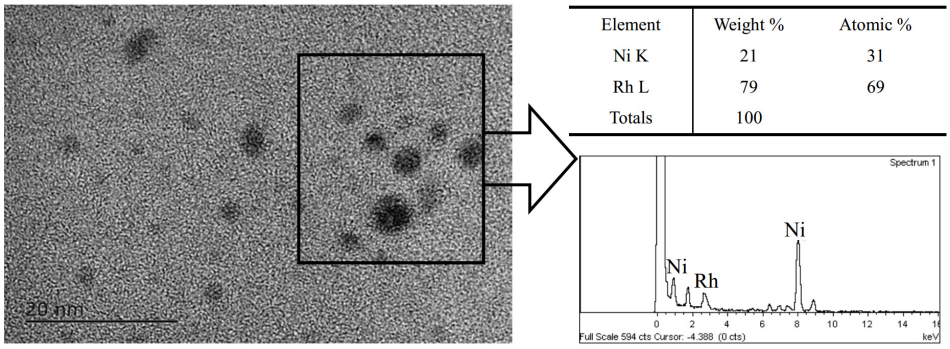

(**a**) TEM (**b**) EDS

Figure 3. TEM image (**a**) and mapping–EDS (**b**) of $Rh_{70}Ni_{30}$ BNPs (R_{ISO} = 40, C_{Metal} = 0.66 mM, reduced under ice–water bath for 1h).

In order to further verify the formation of an alloyed structure in the as–prepared BNPs, a lattice fringes analysis was also carried out, based on high–resolution transmission electron microscopy (HRTEM) images of the $Rh_{70}Ni_{30}$ colloidal dispersions. The particles exhibit an obvious crystalline structure, as revealed in Figure 4. The interplanar distances of three individual randomly–chosen particles of $Rh_{70}Ni_{30}$ BNPs were respectively measured to be 0.212 nm (particle–1), 0.218 nm (particle–2), and 0.216 nm (particle–3), as labeled in Figure 4. Comparing the results of Figure 4 with the theoretically interplanar spacing of Rh and Ni (based on XRD standard card, as shown in Table 1), the formation of individual Rh and Ni MNPs in the as–prepared samples can be ruled out. This is due to the mismatch of interplanar distances between these BNPs and Rh, or Ni MNPs. However, it should be noted that the measured interplanar distances lie between the interplanar spacing of Rh (111) (0.2196 nm), and that of Ni (111) (0.2034 nm), as shown in Table 2. This suggests that alloy structures are formed in the particles and the interplanar spacing can be assigned to (111) of the alloy–structured Rh/Ni BNPs. To the best of our knowledge, this is the first report on the preparation of ISOBAM–104 protected alloy–structured Rh/Ni BNPs by using such a facile co–reduction method.

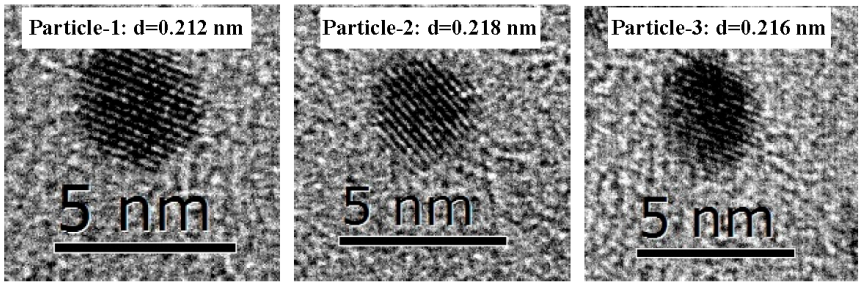

Figure 4. High–resolution transmission electron microscopy (HRTEM) image of as–prepared $Rh_{70}Ni_{30}$ BNPs (R_{ISO} = 40, C_{Metal} = 0.66 mM, reduced under ice–water bath for 1h).

Table 1. Lattice spacing (nm) and indexed reflection planes of Rh and Ni.

Interplanar Face / Element	(111)	(200)	(220)	(311)	(222)	(400)
Rh (ICCD 00–005–0685)	0.2196	0.1902	0.1345	0.1147	0.1098	0.0951
Ni (ICCD 00–004–0850)	0.2034	0.1762	0.1246	0.1062	0.1017	0.0881

Table 2. Lattice spacing (nm) and indexed reflection planes of $Rh_{70}Ni_{30}$ BNPs determined by HRTEM in Figure 4.

Particles	Measured lattice spacing of BNPs	Comparison of lattice spacing of Rh/Ni BNPs with Rh and Ni MNPs	Indexed reflection planes of Rh/Ni BNPs
1	0.212	Between Rh(111) and Ni(111), 0.2196>0.212>0.2034	(111)
2	0.218	Between Rh(111) and Ni(111), 0.2196>0.218>0.2034	(111)
3	0.216	Between Rh(111) and Ni(111), 0.2196>0.216>0.2034	(111)

Catalytic activities of ISOBAM–104 protected $Rh_xNi_{(100-x)}$ (x = 0, 10, 20, 30, 40, 50, 60, 70, 80, 90 and 100) NPs for H_2 generation from hydrolysis of alkaline KBH_4 aqueous solution at 303 K, are illustrated in Figure 5. The activities of BNPs were normalized to mol–H_2·h^{-1}·mol–Rh^{-1} since the catalytic activity of Ni MNPs is very low, showing that most of the Rh/Ni BNPs exhibit higher catalytic activities than that of Rh or Ni MNPs. Moreover, $Rh_{10}Ni_{90}$ BNPs possess the highest catalytic activities with a value of 11,580 mol–H_2·h^{-1}·mol–Rh^{-1} for hydrogen generation, which is respectively about 3 and 37 times higher than that of Rh (3560 mol–H_2·h^{-1}·mol–Rh^{-1}) and Ni MNPs (310 mol–H_2·h^{-1}·mol–Ni^{-1}).

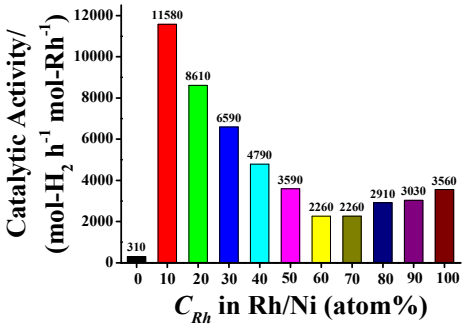

Figure 5. Comparison of catalytic activities of $Rh_{(100-x)}Ni_x$ BNPs with Rh and Ni MNPs (x = 0, 10, 20, 30, 40, 50, 60, 70, 80, 90 and 100) and NPs (R_{ISO} = 40, C_{Metal} = 0.66 mM, reduced under ice–water bath for 1 h; pH = 12 for H_2 generation, 30 °C. The activities of Ni MNPs were normalized to mol–H_2·h^{-1}·mol–Ni^{-1}).

2.2. Kinetic Study on $Rh_{10}Ni_{90}$ BNPs

The effects of pH and reaction temperature on the catalytic activities of the as–prepared BNPs were also investigated using $Rh_{10}Ni_{90}$ as model catalysts. It shows that the final hydrogen productivity of the BNPs decreases from 80% to 45%, with pH increasing from 12 to 14, as shown in Figure 6.

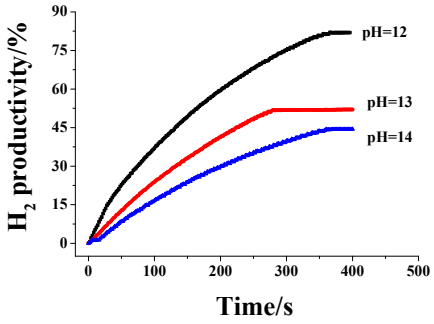

Figure 6. Evaluation of H_2 productivity with reaction time of $Rh_{10}Ni_{90}$ BNPs at different pH values (R_{ISO} = 40, C_{Metal} = 0.66 mM, reduced under ice–water bath for 1h; 30°C).

The apparent activation energy (E_a) of the BNPs for hydrogen generation from the hydrolysis of alkaline KBH_4 solution was calculated by using the Arrhenius method [9,17,27]. The catalytic activities of $Rh_{10}Ni_{90}$ were enhanced with the increasing reaction temperature, and a linear dependence between catalytic rates (in a logarithmic scale, ln k) and the reciprocals of temperature was observed (as shown in Figure 7). According to the Arrhenius equation, the slope of the linear plot is $-E_a/R$, where R represents the universal gas constant. Within the temperatures ranging from 303 to 323 K, E_a was calculated to be 47.2 ± 2.1 kJ/mol for $Rh_{10}Ni_{90}$ BNPs. These results suggest that the as–prepared $Rh_{10}Ni_{90}$ BNPs are excellent catalysts for the hydrolysis of KBH_4 because of their lower apparent activation energy compared with other reported catalysts, such as 51.2kJ/mol for Co–La–Zr–B NPs [28], 52.0kJ/mol for Co–α–Al_2O_3–Cu catalysts [29], 55.6 kJ/mol for Co/alginate hydrogels [30], and 48.8 kJ/mol for Mo incorporated Co–Ru–B catalysts [31], etc.

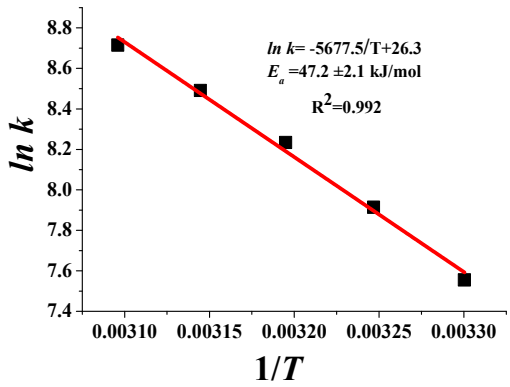

Figure 7. Linear fit of ln$k$ to $1/T$ of $Rh_{10}Ni_{90}$ catalyst for hydrogen generation from KBH_4 (R_{ISO} = 40, C_{Metal} = 0.66 mM, reduced under ice–water bath for 1h; pH = 12 for H_2 generation, 30°C).

2.3. Correlation between Catalytic Activities of the Rh/Ni BNPs and Their Electronic Properties

Figure 5 showed that most of the as–prepared BNPs have higher activity than that of Rh and Ni MNPs, and that $Rh_{10}Ni_{90}$ BNPs possessed the highest catalytic activity for the hydrolysis of KBH_4 among all prepared NPs. According to previous investigations [19,32–34], it is reasonable to suggest that the element components and electronic properties of Rh and Ni atoms affect the catalytic activities of the prepared BNPs. To confirm the existence of electron donation between Rh atoms and Ni atoms,

DFT calculations were carried out to study the electron transfer of the BNPs, and Rh_6Ni_{49} BNP were calculated as a model. The calculation results show that there is indeed an electron charge transfer effect between Rh and Ni atoms. The electron transfers from Rh atoms to Ni atoms owing to the relatively higher electron negativity value of Rh (2.28) than that of Ni (1.91), leading to the presence of negatively–charged Rh atoms and positively–charged Ni atoms in the Rh_6Ni_{49} BNPs (Figure 8). It is believed that the charged Rh and Ni atoms can act as catalytically active sites, and can then enhance the catalytic activities for the hydrogen generation from hydrolysis of KBH_4 aqueous solution [35–38].

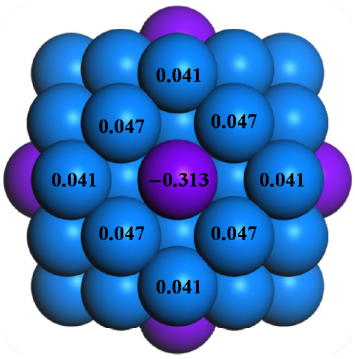

Figure 8. The density functional theory (DFT) calculated Mulliken charge on selected Rh atoms and Ni atoms (blue, Ni; purple, Rh).

3. Experiments

3.1. Raw Materials

Nickel chloride ($NiCl_2 \cdot 6H_2O$, 99.0%, Sinopharm Chemical Reagent Co., Ltd., Shanghai, China), rhodium chloride ($RhCl_3$, 99.9%, Aladdin, Shanghai, China), potassium borohydride (KBH_4, 96.0%, Aladdin, Shanghai, China), and potassium hydroxide (KOH, 96.0%, Aladdin, Shanghai, China) were directly used as raw materials without further purification. ISOBAM–104 (CAS NO. 52032–17–4, chemical structure is shown in Figure 9) was purchased from KURARAY company, Japan. Water was purified by a water distiller system.

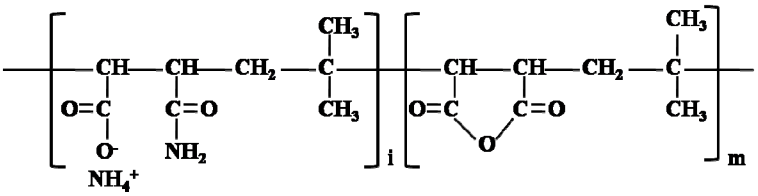

Figure 9. The chemical structure of ISOBAM-104.

3.2. Experiments

A series of $Rh_{(100-x)}Ni_x$ (x = 0, 10, 20, 30, 60, 80, 90, 95 and 100) BNPs were synthesized by changing the addition content of $RhCl_3$ and $NiCl_2$ with the total metal concentration kept at 0.66 mM. Rh/Ni BNPs were prepared through co–reduction method under 273K in N_2 atmosphere. For example, $Rh_{50}Ni_{50}$ BNPs were prepared as follows: 25 mL $RhCl_3$ solution (0.66 mM) and 25 mL $NiCl_2$ solution (0.66 mM) were firstly mixed homogeneously in a two–neck flask under vigorous stirring, and then 50 mL ISOBAM–104 (66 mM) was added into the flask and stirred for another 30 min. Then 10 mL KBH_4 (16.5 mM) was injected into the aqueous solution within 5 s in an ice–water bath [39–41]. The color of the mixed solution slowly changed from transparent to black, which represents the formation of the Rh/Ni BNPs. Finally, colloidal dispersions $Rh_{50}Ni_{50}$ BNPs were obtained after another 1 h of mixing.

3.3. Characterization of Nanoparticles

Ultraviolet and visible light absorption spectra were measured at 200–800 nm by a Shimadzu UV-2550 (Shimadzu company, Japan) recording spectrophotometer. TEM images were taken with a FEI Tecnai G2 50–S–TWIN TEM (FEI company, USA) at the accelerated voltage of 80 kV. The specimens were prepared by placing two or three drops of the prepared colloidal aqueous solution onto a copper microgrid, which was covered with a thin amorphous carbon film, and drying it in air at an ambient temperature. Generally, to evaluate the mean diameter, at least 200 particles from different locations on the grid were selected for each sample. High–resolution transmission electron microscopy (HRTEM) images were observed at the accelerated voltage of 200 kV using a JEM–2100F (JEOL company, Japan) Field Emission High–resolution TEM. The EDS measurement was performed with a NORAN UTW type Si (Li) semiconducting detector attached to the HRTEM equipment.

3.4. Catalytic Properties

The catalytic performance of Rh/Ni BNPs was evaluated by the hydrogen generation from hydrolysis of alkaline KBH_4 aqueous solution. The reaction was started when the alkaline KBH_4 aqueous solution was added into the colloidal catalyst under continuous stirring. Hydrogen was bubbled through the suspension, and its volume was obtained with a water drainage method. At the same time, plots of hydrogen volume vs. reaction time with an interval of 2 s were collected by a computer. The turnover frequency (TOF) was calculated through the slope of a fitted straight line using H_2 volume vs. reaction time curve. The initial specific activities (mol–H_2·h^{-1}·mol–Rh^{-1}) related to the noble metal content of the catalysts were calculated for comparison. Every experiment was repeated at least twice, and the mean value of the measuring results was used for calculating the value of TOF. The catalytic kinetics were investigated at varied pH (12, 13 and 14, 303 K) and different temperatures (303 K, 308 K, 313 K, 318 K and 323 K, pH = 12), using $Rh_{10}Ni_{90}$ as model catalysts.

3.5. DFT Calculation

DFT calculations were carried out using spin–polarization DFT/GGA with the PBE exchange–correlation functional [42], as implemented in the $DMol^3$ package [43] (BIOVIA company, San Diego, CA, USA). Double numerical basis set and polarization functions were carried out to describe the valence electrons, and an electron relativistic core treatment was used to perform full optimization of the investigated cluster model of Rh_6Ni_{49} BNP without symmetry constraint. The convergence criteria were set to medium quality with a tolerance for self–consistent field (SCF), optimization energy, maximum force, and maximum displacement of 10^{-5} Ha, 2×10^{-5} Ha, 0.004 Ha/Å and 0.005 Å, respectively. Charge analysis was performed on the basis of the Mulliken population distribution scheme [44,45].

4. Conclusions

ISOBAM–104 protected alloy–structured Rh/Ni BNPs were prepared by a co–reduction method and characterized by UV–Vis, TEM, EDS and HRTEM. The catalytic activities and kinetic study for KBH_4 hydrolysis reaction were also investigated. The as–prepared Rh/Ni BNPs possessed high catalytic activities, and the activities of the $Rh_{10}Ni_{90}$ BNPs with an average size of 3 nm were higher than that of Ni MNPs. They were also higher than that of the Rh MNPs, even though the latter has a much smaller size of 1.9 nm. The apparent activation energy was calculated to be 47.2 ± 2.1 kJ/mol for $Rh_{10}Ni_{90}$ BNPs, which is lower than that of most reported catalysts, suggesting that Rh/Ni BNPs with low Rh loading were excellent catalysts for the hydrolysis of KBH_4. The high catalytic activities of Rh/Ni BNPs could be attributed to the existence of the electron transfer effects between Rh and Ni atoms of the BNPs, which was confirmed by the DFT calculation. The enhanced performance of Rh/Ni BNPs is of major importance towards the direct production of H_2 through hydrolysis of KBH_4.

Acknowledgments: This work was financially supported by the National Natural Science Foundation of China (Grant No. 5142184 and 51672194), and Program for Innovative Teams of Outstanding Young and Middle–aged Researchers in the Higher Education Institutions of Hubei Province (T201602).

Author Contributions: Haijun Zhang conceived and designed the experiment. Liqiong Wang, Chengpeng Jiao performed catalysts synthesis, whereas Zili Huang, Feng Liang, Simin Liu and Yuhua Wang carried out catalyst characterization and evaluation. Liqiong Wang, Liang Huang and Haijun Zhang contributed with the analysis and interpretation of characterization results. All authors discussed the results and approved the final version of the manuscript.

Conflicts of Interest: The authors declare no conflict of interest.

References

1. Chu, D.M.; Zhang, C.Y.; Yang, P.; Du, Y.K.; Lu, C. WS_2 as an effective noble–Metal free cocatalyst modified $TiSi_2$ for enhanced photocatalytic hydrogen evolution under visible light irradiation. *Catalysts* **2016**, *6*, 136–147. [CrossRef]
2. Konsolakis, M.; Ioakimidis, Z.; Kraia, T.; Marnellos, G.E. Hydrogen production by ethanol steam reforming (ESR) over CeO_2 supported transition metal (Fe, Co, Ni, Cu) catalysts: Insight into the structure–Activities relationship. *Catalysts* **2016**, *6*, 39. [CrossRef]
3. Zhang, F.C.; Chen, R.; Zhang, W.H.; Zhang, W.B. A Ti–Decorated boron monolayer: A promising material for hydrogen storage. *RSC Adv.* **2016**, *6*, 12925–12931. [CrossRef]
4. Wang, L.; Zhang, T.; He, H.Q.; Zhang, J.L. Mechanism for H_2 release from potential hydrogen storage materials of phosphine alane and phosphine borane in the presence or absence of alane or borane: A theoretical study. *RSC Adv.* **2013**, *3*, 21949–21958. [CrossRef]
5. Yadav, M.; Xu, Q. Liquid–phase chemical hydrogen storage materials. *Energy Environ. Sci.* **2012**, *5*, 9698–9725. [CrossRef]
6. Jiang, H.L.; Singh, S.K.; Yan, J.M.; Zhang, X.B.; Xu, Q. Liquid–phase chemical hydrogen storage: Catalytic hydrogen generation under ambient conditions. *ChemSusChem.* **2010**, *3*, 541–549. [CrossRef] [PubMed]
7. Wang, S.B.; Xin, X.; Zhang, H.; Shen, J.L.; Zheng, Y.; Song, Z.H.; Yang, Y.Z. Stable monodisperse colloidal spherical gold nanoparticles formed by an imidazolium gemini surfactant–based water–in–oil microemulsion with excellent catalytic performance. *RSC Adv.* **2016**, *6*, 28156–28164. [CrossRef]
8. Jia, H.; Gao, X.P.; Chen, Z.L.; Liu, G.Q.; Zhang, X.; Yan, H.; Zhou, H.T.; Zheng, L.Q. The high yield synthesis and characterization of gold nanoparticles with superior stability and their catalytic activities. *Cryst. Eng. Commun.* **2012**, *14*, 7600–7606. [CrossRef]
9. Jiao, C.P.; Huang, Z.L.; Wang, X.F.; Zhang, H.J.; Lu, L.L.; Zhang, S.W. Synthesis of Ni/Au/Co trimetallic nanoparticles and their catalytic activities for hydrogen generation from alkaline sodium borohydride aqueous solution. *RSC Adv.* **2015**, *5*, 34364–34371. [CrossRef]
10. Seven, F.; Sahiner, N. Enhanced catalytic performance in hydrogen generation from $NaBH_4$ hydrolysis by super porous cryogel supported Co and Ni catalysts. *J. Power Sour.* **2014**, *272*, 128–136. [CrossRef]
11. Wu, C.; Bai, Y.; Liu, D.X.; Wu, F.; Pang, M.L.; Yi, B.L. Ni–Co–B catalyst–promoted hydrogen generation by hydrolyzing $NaBH_4$ solution for in situ hydrogen supply of portable fuel cells. *Catal. Today* **2011**, *170*, 33–39. [CrossRef]
12. Wang, X.F.; Sun, S.R.; Huang, Z.L.; Zhang, H.J.; Zhang, S.W. Preparation and catalytic activities of PVP–protected Au/Ni bimetallic nanoparticles for hydrogen generation from hydrolysis of basic $NaBH_4$ solution. *Int. J. Hydrog. Energy* **2014**, *39*, 905–916. [CrossRef]
13. Wang, X.F.; Huang, Z.L.; Lu, L.L.; Zhang, H.J.; Cao, Y.N.; Gu, Y.J.; Cheng, Z.; Zhang, S.W. Preparation and Catalytic Activities of Au/Co Bimetallic Nanoparticles for Hydrogen Generation from $NaBH_4$ Solution. *J. Nanosci. Nanotechnol.* **2015**, *15*, 2770–2776. [CrossRef] [PubMed]
14. Yang, X.J.; Cheng, F.Y.; Liang, J.; Tao, Z.L.; Chen, J. Pt_xNi_{1-x} nanoparticles as catalysts for hydrogen generation from hydrolysis of ammonia borane. *Int. J. Hydrog. Energy* **2009**, *34*, 8785–8791. [CrossRef]
15. Wang, H.L.; Yan, J.M.; Wang, Z.L.; Jiang, Q. One–step synthesis of Cu@FeNi core–shell nanoparticles: Highly active catalyst for hydrolytic dehydrogenation of ammonia borane. *Int. J. Hydrog. Energy* **2012**, *37*, 10229–10235. [CrossRef]

16. Pan, Y.; Zhang, F.; Wu, K.; Lu, Z.Y.; Chen, Y.; Zhou, Y.M.; Tang, Y.W.; Lu, T.H. Carbon supported Palladium–Iron nanoparticles with uniform alloy structure as methanol–tolerant electrocatalyst for oxygen reduction reaction. *Int. J. Hydrog. Energy* **2012**, *37*, 2993–3000. [CrossRef]
17. Zhang, H.J.; Deng, X.G.; Jiao, C.P.; Lu, L.L.; Zhang, S.W. Preparation and catalytic activities for H_2O_2 decomposition of Rh/Au bimetallic nanoparticles. *Mater. Res. Bull.* **2016**, *79*, 29–35. [CrossRef]
18. Zhang, H.J.; Cao, Y.N.; Lu, L.L.; Cheng, Z.; Zhang, S.W. Trimetallic Au/Pt/Rh nanoparticles as highly active catalysts for aerobic glucose oxidation. *Metall. Mater. Trans. B* **2014**, *46*, 523–530. [CrossRef]
19. Zhang, H.J.; Watanabe, T.; Okumura, M.; Haruta, M.; Toshima, N. Catalytically highly active top gold atom on palladium nanocluster. *Nat. Mater.* **2012**, *11*, 49–52. [CrossRef] [PubMed]
20. Larichev, Y.V.; Netskina, O.V.; Komova, O.V.; Simagina, V.I. Comparative XPS study of Rh/Al_2O_3 and Rh/TiO_2 as catalysts for $NaBH_4$ hydrolysis. *Int. J. Hydrog. Energy* **2010**, *35*, 6501–6507. [CrossRef]
21. Jacinto, M.J.; Kiyohara, P.K.; Masunaga, S.H.; Jardim, R.F.; Rossi, L.M. Recoverable rhodium nanoparticles: Synthesis, characterization and catalytic performance in hydrogenation reactions. *Appl. Catal. A Gen.* **2008**, *338*, 52–57. [CrossRef]
22. Rakap, M. PVP–stabilized Ru–Rh nanoparticles as highly efficient catalysts for hydrogen generation from hydrolysis of ammonia borane. *J. Alloys Compd.* **2015**, *649*, 1025–1030. [CrossRef]
23. Li, C.M.; Dou, Y.B.; Liu, J.; Chen, Y.D.; He, S.; Wei, M.; Evans, D.G.; Duan, X. Synthesis of supported Ni@(RhNi–alloy) nanocomposites as an efficient catalyst towards hydrogen generation from $N_2H_4BH_3$. *Chem. Commun.* **2013**, *49*, 9992–9994. [CrossRef] [PubMed]
24. Ferencz, Z.; Erdőhelyi, A.; Baán, K.; Oszkó, A.; Óvári, L.; Kónya, Z.; Papp, C.; Steinrück, H.P.; Kiss, J. Effects of support and Rh additive on Co–based catalysts in the ethanol steam reforming reaction. *ACS Catal.* **2014**, *4*, 1205–1218. [CrossRef]
25. Varga, E.; Baán, K.; Samu, G.F.; Erdőhelyi, A.; Oszkó, A.; Kónya, Z.; Kiss, J. The Effect of Rh on the Interaction of Co with Al_2O_3 and CeO_2 Supports. *Catal. Lett.* **2016**, *146*, 1800–1807. [CrossRef]
26. Arbag, H.; Yasyerli, S.; Yasyerli, N.; Dogu, G. Activities and stability enhancement of Ni–MCM–41 catalysts by Rh incorporation for hydrogen from dry reforming of methane. *Int. J. Hydrog. Energy* **2010**, *35*, 2296–2304. [CrossRef]
27. Zhang, H.J.; Li, W.Q.; Gu, Y.J.; Zhang, S.W. Preparation and Catalytic Activities of Poly(*N*–vinyl–2–pyrrolidone)–Protected Au nanoparticles for the aerobic oxidation of glucose. *J. Nanosci. Nanotechnol.* **2014**, *14*, 5743–5751. [CrossRef] [PubMed]
28. Loghmani, M.H.; Shojaei, A.F. Hydrogen production through hydrolysis of sodium borohydride: Oleic acid stabilized Co–La–Zr–B nanoparticle as a novel catalyst. *Energy* **2014**, *68*, 152–159. [CrossRef]
29. Chamoun, R.; Demirci, U.B.; Zaatar, Y.; Khoury, A.; Miele, P. Co–αAl_2O_3–Cu as shaped catalyst in $NaBH_4$ hydrolysis. *Int. J. Hydrog. Energy* **2010**, *35*, 6583–6591. [CrossRef]
30. Ai, L.H.; Gao, X.Y.; Jiang, J. In situ synthesis of cobalt stabilized on macroscopic biopolymer hydrogel as economical and recyclable catalyst for hydrogen generation from sodium borohydride hydrolysis. *J. Power Sour.* **2014**, *257*, 213–220. [CrossRef]
31. Wang, W.L.; Zhao, Y.C.; Chen, D.H.; Wang, X.; Peng, X.L.; Tian, J.N. Promoted Mo incorporated Co–Ru–B catalyst for fast hydrolysis of $NaBH_4$ in alkaline solutions. *Int. J. Hydrog. Energy* **2014**, *39*, 16202–16211. [CrossRef]
32. Zhang, H.J.; Lu, L.L.; Kawashima, K.; Okumura, M.; Haruta, M.; Toshima, N. Synthesis and catalytic activities of crown jewel–structured (IrPd)/Au trimetallic nanoclusters. *Adv. Mater.* **2015**, *27*, 1383–1388. [CrossRef] [PubMed]
33. Zhang, H.J.; Toshima, N. Synthesis of Au/Pt bimetallic nanoparticles with a Pt–rich shell and their high catalytic activities for aerobic glucose oxidation. *J. Colloid Interface Sci.* **2013**, *394*, 166–176. [CrossRef] [PubMed]
34. Zhang, H.J.; Okumura, M.; Toshima, N. Stable Dispersions of PVP–protected Au/Pt/Ag trimetallic nanoparticles as highly active colloidal catalysts for aerobic glucose oxidation. *J. Phys. Chem. C* **2011**, *115*, 14883–14891. [CrossRef]
35. Zhang, H.J.; Toshima, N. Crown Jewel–structured Au/Pd nanoclusters as novel catalysts for aerobic glucose oxidation. *J. Nanosci. Nanotechnol.* **2013**, *13*, 5405–5412. [CrossRef] [PubMed]
36. Zhang, H.J.; Watanabe, T.; Okumura, M.; Haruta, M.; Toshima, N. Crown Jewel catalyst: How neighboring atoms affect the catalytic activities of top Au atoms? *J. Catal.* **2013**, *305*, 7–18. [CrossRef]

37. Zhang, H.J.; Kawashima, K.; Okumura, M.; Toshima, N. Colloidal Au single–atom catalysts embedded on Pd nanoclusters. *J. Mater. Chem. A* **2014**, *2*, 13498–13508. [CrossRef]
38. Zhang, H.J.; Wang, L.Q.; Lu, L.L.; Toshima, N. Preparation and catalytic activities for aerobic glucose oxidation of Crown Jewel structured Pt/Au bimetallic nanoclusters. *Sci. Rep.* **2016**, *6*, 30752–30762. [CrossRef] [PubMed]
39. Zhang, H.J.; Haba, M.; Okumura, M.; Akita, T.; Hashimoto, S.; Toshima, N. Novel formation of Ag/Au bimetallic nanoparticles by physical mixture of monometallic nanoparticles in dispersions and their application to catalysts for aerobic glucose oxidation. *Langmuir* **2013**, *29*, 10330–10339. [CrossRef] [PubMed]
40. Zhang, H.J.; Toshima, N. Fabrication of catalytically active AgAu bimetallic nanoparticles by physical mixture of small Au clusters with Ag ions. *Appl. Catal. A* **2012**, *447–448*, 81–88. [CrossRef]
41. Zhang, H.J.; Toshima, N. Preparation of novel Au/Pt/Ag trimetallic nanoparticles and their high catalytic activities for aerobic glucose oxidation. *Appl. Catal. A* **2011**, *400*, 9–13. [CrossRef]
42. Brajczewska, M.; Vieira, A.; Fiolhais, C.; Perdew, J.P. Volume shift and charge instability of simple–metal clusters. *Prog. Surf. Sci.* **1996**, *53*, 305–313. [CrossRef]
43. Delley, B. DMol^3 DFT studies: From molecules and molecular environments to surfaces and solids. *Comput. Mater. Sci.* **2000**, *17*, 122–126. [CrossRef]
44. Reed, A.E.; Weinstock, R.B.; Weinhold, F. Natural population analysis. *J. Chem. Phys.* **1985**, *83*, 735–746. [CrossRef]
45. Clark, A.E.; Sonnenberg, J.L.; Hay, P.J.; Martin, R.L. Density and wave function analysis of actinide complexes: What can fuzzy atom, atoms–in–molecules, Mulliken, Löwdin, and natural population analysis tell us? *J. Chem. Phys.* **2004**, *121*, 2563–2570. [CrossRef] [PubMed]